Research Square

Preprints are preliminary reports that have not undergone peer review.
They should not be considered conclusive, used to inform clinical practice,
or referenced by the media as validated information.

A Wheatstone Bridge-Inspired Microfluidic Trap For Precise Tuning of the Content of an Immobilized Droplet

Damian Zaremba

dzaremba@ippt.pan.pl

Institute of Fundamental Technological Research Polish Academy of Sciences https://orcid.org/0000-0001-9055-4960

Barbara Kupikowska-Stobba

Institute of Fundamental Technological Research Polish Academy of Sciences

Slawomir Blonski

Institute of Fundamental Technological Research Polish Academy of Sciences

Piotr Korczyk

Institute of Fundamental Technological Research Polish Academy of Sciences

Article

Keywords:

Posted Date: September 9th, 2026

DOI: https://doi.org/10.21203/rs.3.rs-10460249/v1

License: This work is licensed under a Creative Commons Attribution 4.0 International License.
Read Full License

Additional Declarations: There is no conflict of interest

A Wheatstone Bridge-Inspired Microfluidic Trap For Precise Tuning of the Content of an Immobilized Droplet

Damian Zaremba,*[a] Barbara Kupikowska-Stobba,[a] Slawomir Blonski,[a] and Piotr M. Korczyk[a]

a. Institute of Fundamental Technological Research, Polish Academy of Sciences, Pawinskiego 5B, 02-106 Warsaw, Poland

official e-mails: dzaremba@ippt.pan.pl, bstobba@ippt.pan.pl, sblonski@ippt.pan.pl, pkor@ippt.pan.pl

* corresponding author, secondary e-mail: dzarembad@gmail.com, phone number: +48 797 111 828

Abstract

We present a novel droplet-based microfluidic trap, inspired by the Wheatstone bridge in electronics, that can immobilize a droplet at least an order of magnitude larger than the carrier droplets used in a microfluidic network. With each incoming carrier droplet, the trap performs automated, high-precision medium exchange via a programmable coalescence-and-displacement mechanism, thereby maintaining the volume of the immobilized droplet constant. This mechanism also enables precise delivery of a wide range of chemical or biological factors, ensures tight control over the droplet's chemical composition, or allows the propagation of a concentration wave within the droplet. We demonstrate the design's versatility by presenting not only basic construction but also modifications that enhance mixing within the immobilized droplet or create a hydrophilic bottom to enable adhesive cell cultures. We present preliminary biological experiments conducted in the microfluidic trap using Escherichia coli and A549 epithelial cells as model organisms, demonstrating the proposed system's potential for biomedical applications.

Introduction

Microfluidic chips offer unique advantages over their macroscale counterparts, primarily by using microchannels comparable in size to individual cell diameters, enabling real-time, high-resolution monitoring of single cells. Most current microfluidic strategies employ single-phase systems where a continuous aqueous phase flows through the chip in an open-loop configuration.[1–7] Platforms such as VersaLive have demonstrated the versatility of these systems for mammalian cell culture,[8] enabling protocols for time-lapse imaging,[9] immunostaining,[10] and even transfection.[11] However, the lack of physical compartmentalization,[12] renders single-phase systems susceptible to biofouling,[13] non-specific protein adsorption onto channel walls,[14] and cross-contamination between experimental runs. These limitations pose significant barriers to the clinical translation of microfluidic technologies, as protein adsorption can alter medium composition over time and ultimately lead to channel occlusion.[14,15]

Droplet-based, two-phase microfluidics offer a robust alternative by confining cells within discrete microdroplets of culture medium separated by an immiscible, biocompatible oil phase. This compartmentalization effectively isolates a cell suspension from the channel walls, preventing uncontrolled adhesion, cross-contamination, and protein adsorption while enabling precise dosing of minute reagent

volumes.[16–21] One of the most significant advantages of this approach is the acceleration of secreted metabolite accumulation within minute pico- to microliter droplet volumes,[16] enabling the rapid detection of biologically relevant compounds for time-sensitive applications such as cancer diagnostics[22] and pathogen detection.[23] However, this “microreactor” effect also poses limitations: although isolation enhances detection sensitivity, confinement to extremely small volumes results in rapid nutrient depletion and acidification,[24] typically limiting culture viability to approximately 72 h.[25]

Efforts to solve this limitation have generally followed two paths. The first involves circulating droplets through a complex microfluidic network, periodically merging them with fresh medium droplets.[21,26] While robust, this method involves intricate optical feedback loops and exposes cells to elevated shear stress at the droplet periphery.[27] Such excessive stress can impair critical phenotypic maturation and disrupt cellular organization. The second path involves immobilizing droplets on-chip using microfluidic traps,[28] where the cell-laden droplet remains stationary while exchange occurs via controlled coalescence. Previous attempts at stationary trapping, such as those by Jin et al.[29] using adhesion sites or Totlani et al.[30,31] using cup-shaped traps, have struggled with the lack of an efficient outflow mechanism. Without a way to remove spent medium, these systems suffer from waste accumulation and poor volume control, often relying on passive overflow, which results in incremental dilution.

The device presented in this study overcomes these issues by introducing a novel microfluidic trap that can form and stably immobilize a large, stationary droplet (several hundred nanoliters in volume). Inspired by a Wheatstone bridge, the trap is designed with modular microfluidic geometries to perform specific functional roles within a complex microfluidic network.[32,33] The architecture enables a unique coalescence-displacement process: as incoming fresh medium droplets merge with the stationary droplet, an equal volume of spent medium is simultaneously displaced and expelled. This mechanism ensures a constant droplet volume while maintaining continuous nutrient replenishment and waste removal without subjecting the encapsulated cells to excessive mechanical forces.

In the present investigation, we focused on the technical aspects of the developed microfluidic trap and explored the physical principles, mass-transfer mechanisms, and flow dynamics. To demonstrate the high potential of the microfluidic trap in biomedical applications, we conducted preliminary experiments to evaluate its ability to support the growth of both rapidly proliferating bacteria (*Escherichia coli*) and adherent mammalian cells (A549 epithelial cells). These preliminary proof-of-concept tests lay the groundwork for further, more focused studies on cultivating different cell types with distinct nutritional and mechanical requirements in the presented microfluidic trap. Moreover, by enabling automated, sustained perfusion of stationary culture droplets and precise dosing of minute reagent volumes at the nanoliter scale, the presented system has the potential to address a longstanding limitation of current droplet culture systems and to open new possibilities for precisely controlled experiments in droplet microfluidic platforms.

Results

Design description of the microfluidic trap

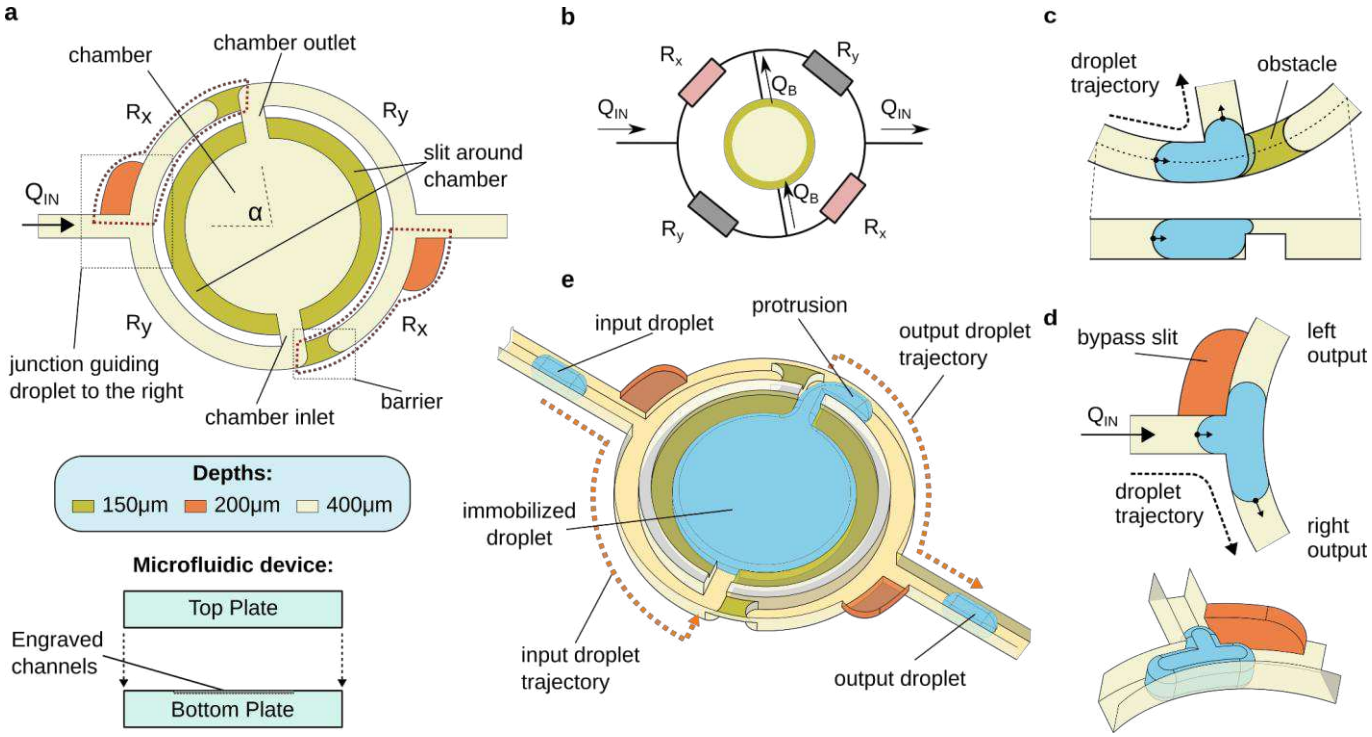


Fig. 1. *Basic design of the Wheatstone bridge-inspired microfluidic trap: a) A top-down view of the microfluidic trap design engraved into the bottom plate of the microfluidic device with channel depths indicated. b) Functional analogy of the chamber represented as a Wheatstone bridge electrical circuit, where the Q_{IN} corresponds to the input flow (Q_{CP} + Q_{DP}) and the Q_B corresponds to the bridge flows. Panels c) and d) show magnified views of the barrier structure and the junction directing the droplets to the right, respectively. e) A perspective view of the microfluidic trap highlighting the droplet trajectories.*

The Wheatstone bridge is a well-known electrical circuit composed of four resistors arranged in two parallel branches, each containing two resistors connected in series. A fifth resistor is connected between the series connections in each branch, forming a bridge between them. When the resistances in the two branches are unbalanced, a current flows through the bridge. When balanced, the circuit produces a zero voltage difference and no current flows.

Drawing on this analogy, we designed a microfluidic trap shown in Fig. 1a and e, in which the 3.0 mm-diameter chamber (of arbitrary depth limited by the thickness of the PC plate) serves as a bridge that traps a large droplet. The chamber is positioned within the loop of microchannels, each with a cross-section of 0.4 mm × 0.4 mm, allowing the CP to bypass the chamber. In addition, the chamber is surrounded by additional slits, each 0.15 mm high and 0.2 mm wide. The primary function of the slits is to allow the CP to flow around the central part through the slits when the chamber is filled with the DP. The slits enable the immobilized droplet to attain an optimal shape relative to the chamber geometry, while the flow of the surrounding CP induces gentle internal circulation within the droplet.

According to the well-established analogy between laminar fluid flow and Ohm's law,[34] we use the fact that

the Wheatstone bridge can be balanced to minimize the pressure drop across the bridge and, consequently, reduce the corresponding flow rate, denoted as in Fig. 1b. The device exhibits rotational symmetry about its center. Using the notations of channel resistances R_x and R_y, as shown in Fig. 1b, a calculation reveals that the bridge achieves a balanced state when R_x=R_y.

The channel denoted as R_x contains an obstacle (see Fig. 1c) positioned at its junction with the chamber inlet or outlet (see Fig. 1a). The obstacle at the chamber entrance allows the CP to flow freely toward the channel while directing droplets into the chamber inlet. The obstacle at the chamber outlet, on the other hand, primarily serves to maintain design symmetry and facilitate uniform CP flow distribution throughout the microfluidic network.

By manipulating the angle of the bridge and analyzing single-phase μPIV within the chamber, we determined that a near-perfect balance is achieved when α lies between 80° and 90° (see Fig. S5). However, achieving complete balance was not our goal. Instead, we selected an angle of 80° for subsequent experiments, leaving the bridge intentionally slightly unbalanced. This design permits a weak compensating flow through the bridge, sufficient to prevent droplet displacement across a wide range of operating conditions (flow rates up to Q_{CP} = 10 mL h^{-1} for dyed water used as the DP). During the system preparation, when an air bubble forms inside the chamber, this slight imbalance enables its removal at higher flow rates.

Another critical component integrated into the loop surrounding the chamber, essential for the proper function of the trap, is the bifurcating junction with a bypass slit.[33] This feature ensures that droplets enter the correct branch of the loop and prevents the splitting of elongated droplets between the two bifurcations (see Fig. 1d). In our previous work,[33] we showed that while this Y-junction has little influence on the distribution of single-phase flows, it markedly affects droplet flows across a wide range of flow-rate ratios between the two outlets. As with the obstacle placed at the chamber outlet, the bypass slit at the loop's output was incorporated to maintain symmetry and allow trap operation when reverse CP flow is used.

Principles of operation and manipulation of the immobilized droplet contents

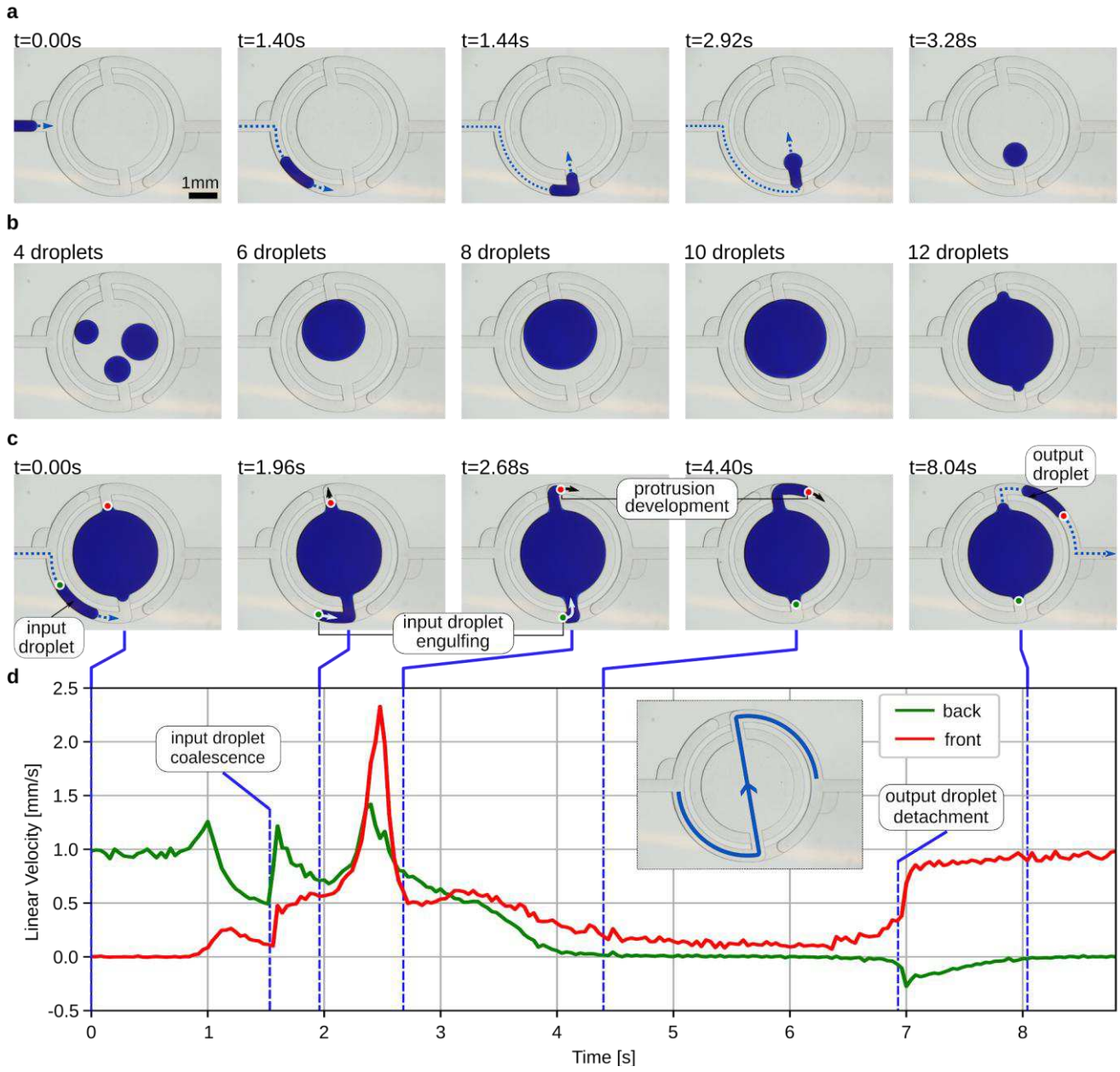


Fig. 2. *Principles governing the operation of the microfluidic trap (see Movie 1) with a chamber depth of 0.4 mm. a) A series of snapshots showing the introduction of the first droplet to the initially empty chamber. b) Gradual filling of the chamber with a series of droplets that coalesce inside the chamber. The selected images show the microfluidic trap after introducing 4, 6, 8, 10, and 12 droplets. Note that 12 droplets fill the entire chamber. c) A series of snapshots illustrating the fusion of the input droplet with the immobilized droplet, which initiates the release of the output droplet. d) Estimation of the linear velocity at two extreme points along the path marked in the inset image: i) the back of the input droplet (and later the back of the immobilized droplet after coalescence) and ii) the front of the immobilized droplet (and later the front of the output droplet after its detachment). The back and front are marked with colored circles in the snapshots shown in (c). The velocity was estimated along the path marked in the inset. The path follows the general direction of DP flow through the trap.*

Initially, the device is filled with the CP, after which the DP is introduced as a train of droplets entering the

input channel. Within the chamber, the droplet drifts under weak flow and assumes a round shape (see the last snapshot in Fig. 2a). The subsequent droplets follow the same trajectory and coalesce with the previously introduced droplets, gradually forming a growing droplet within the chamber (see Fig. 2b). This resulting droplet continues to expand until it fills the entire volume of the chamber, which measures 2.8 µL for a chamber height of h = 0.4 mm (see the last image in Fig. 2b). As a result, the chamber becomes fully occupied by a single large medium droplet (referred to as the immobilized droplet). Once the chamber is filled, the volume of the immobilized droplet can no longer increase because it occupies all available space.

After the chamber is filled, each subsequent input droplet follows the same trajectory and is guided toward the chamber, where it merges with the immobilized droplet (see Fig. 2c). Upon merging (t=1.96 s), the immobilized droplet becomes temporarily overloaded, producing a shrinking residual tail at the chamber inlet and a protrusion at the chamber outlet; together, these features disturb the local CP flow in the opposite loop branches and intermittently increase the hydraulic resistance. Under these unstable conditions, the DP is driven across the chamber from the inlet to the outlet (i.e., translational motion of the DP), thereby advancing the front of the immobilized droplet and enlarging the outlet protrusion until it detaches as an output droplet (see Fig. 2c; t = 2.68–4.40 s). During this brief period, the main motion follows the trajectory schematically shown in the inset of Fig. 2d. If we use long carrier droplets that, at the same time, the protrusion and tail block both obstacles, the transient change in the flow configuration is reflected by the peak in the plot (see Fig. 2d; between t = 1.96 s and t = 2.68 s) that should represent the flow through the chamber close to Q_{IN}. The volume of the expelled output droplet matches that of the incoming input droplet, thereby maintaining an essentially constant volume of the immobilized droplet. We refer to this sequence as the translational flow mode, which constitutes the mechanism responsible for controlled mass exchange within the immobilized droplet.

The immobilized droplet's position and volume remain constant despite the passage of successive DP droplets through it. The immobilized droplet is held in place by the difference in interface curvature between its front and back. When the protrusion forms and extends from the immobilized droplet (see Fig. 2c; between t = 4.40 s and t = 8.04 s) but before it detaches, the back of the immobilized droplet exhibits a curvature defined by the chamber ($\kappa_B \approx \frac{2}{W}+\frac{2}{H}= \frac{1}{1.5}mm + \frac{1}{200}um$). The protrusion, in turn, has a curvature determined by the regular channel cross-section ($\kappa_F \approx \frac{1}{200}\mu m+\frac{1}{200}\mu m$).

The pressure difference between the back and front of the immobilized droplet is related to the Laplace pressure and can be estimated as $\Delta P=P_B - P_F=\gamma(\kappa_B - \kappa_F)<0$. A negative pressure difference indicates a tendency for the immobilized droplet to move backward into the chamber. However, the protrusion is cut off by the shear flow generated by the CP in the looping channel, similar to droplet generation at a T-junction. This protrusion detaches, forming an output droplet of the same size as the input droplet (see Fig. 2c; t = 8.04 s). Consequently, the volume of the immobilized droplet remains unchanged after each insertion of an input droplet. Each subsequent input droplet triggers the release of an output droplet of the same size from the chamber.

Flow patterns inside the immobilized droplet

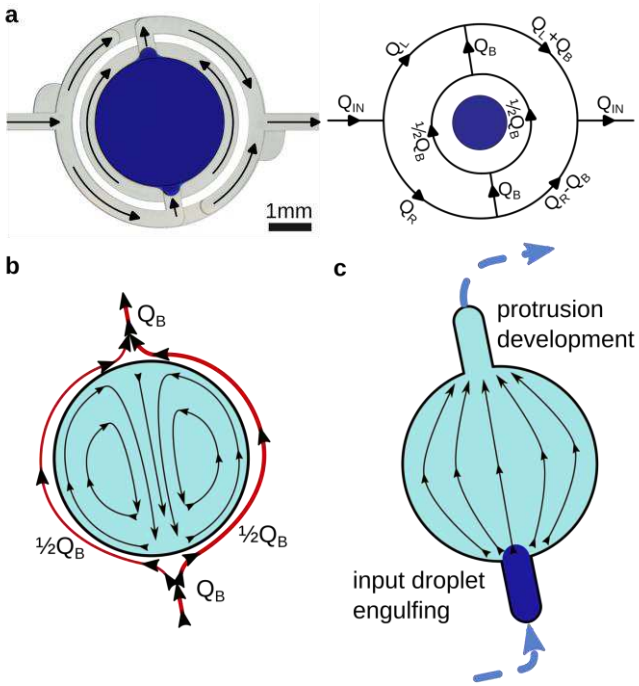


Fig. 3. *Flow patterns within the droplet-based microfluidic trap. a) The primary flow structure generated by the flow of CP around the static droplet. Left: An image of the loaded trap, with arrows indicating the flow direction in the channels. Right: Schematic illustration of the flow distribution in the channel system. The CP flow (Q_{IN}) bifurcates in the channel loop into Q_R and Q_L flows. A portion of the Q_R flow, denoted as the Q_B, enters the chamber and flows through it, bypassing the immobilized droplet via dedicated slits. b) A schematic illustration of the streamlines of the internal circulation within the immobilized droplet, driven by the flow around the droplet according to the configuration shown in a). c) A schematic representation of streamlines during translational flow inside the immobilized droplet, induced by the fusion/fission of small droplets.*

The Wheatstone bridge-like design implies that the main CP flow entering the system bifurcates, circulates through both arms of the loop surrounding the chamber, and then rejoins at the downstream end of the circle (see Fig. 3a). Owing to the imperfect balance of the bridge, a portion of the CP flow (Q_B) enters the chamber and flows through it, bypassing the immobilized droplet via dedicated slits (see Fig. 3b). The flat geometry of the immobilized droplet allows us to focus our analysis on the flows in the device plane.

In circulation mode, the bridge flow Q_B enters the chamber and bifurcates, flowing around the immobilized droplet through the slits (Fig. 3a). This flow close to the droplet surface generates tangential tension on the droplet surface, inducing motion in the same direction on the opposite side of the interface within the droplet surface. Since the droplet is a closed system, this disturbance drives internal circulation (Fig. 3b), thereby facilitating mixing and homogenization of its contents.

Another characteristic flow structure – the translational flow mode – arises precisely when the input droplets are directed into the right arm of the loop and then toward the chamber inlet, where they coalesce with the immobilized droplet. In this mode, the DP flows from the inlet to the outlet through the immobilized droplet. When the immobilized droplet becomes temporarily overloaded (i.e., the input droplet has already

merged, but the output droplet has not yet detached), the excess volume extends into both the inlet and outlet of the chamber, disrupting the CP flow through the bridge (see Fig. 2c). This disturbance interrupts the internal circulation previously described within the immobilized droplet. The gradual engulfment of the input droplet by the immobilized droplet and the simultaneous formation of a protrusion on the opposite side generate translational flow across the immobilized droplet–from the inlet to the outlet (see Fig. 3c).

Mass exchange within the immobilized droplet

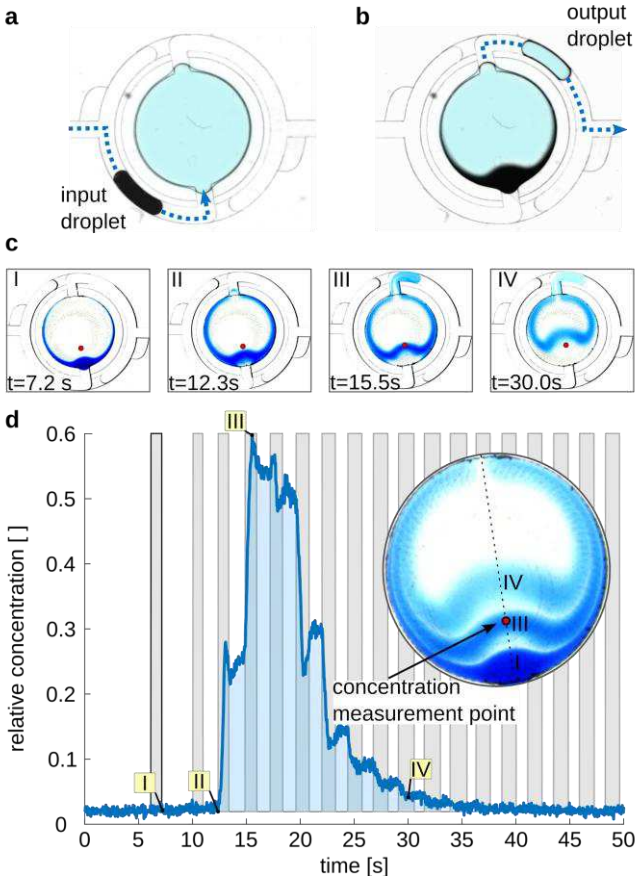


Fig. 4. *Mass exchange and concentration wave propagation in the immobilized droplet. a) Experimental visualization of mass exchange driven by small carrier droplets: the input droplet approaches the immobilized droplet before coalescence. b) Output droplet ejection: the dark region indicates the dye introduced by the input droplet, whereas the light-blue output contains only the original immobilized droplet contents. c) Time-lapse sequence of snapshots (I–IV) showing the immobilized droplet (initially composed of buffer) after the addition of a dye-containing droplet, followed by buffer droplets; each snapshot corresponds to the time points labeled I–IV on the plot in panel d). d) Relative dye concentration over time measured at the position marked in red; gray bars indicate fusion/fission events, with the first event (outlined in black) corresponding to the dye-containing droplet. Inset: composite image of snapshots I, III, and IV from panel c) showing the propagation of the concentration wave across the immobilized droplet.*

Notably, although the volume of the immobilized droplet remains constant after each droplet enters, its contents continue to exchange. While the output droplet removes a portion of the immobilized droplet, the input droplet delivers an equal volume of fresh medium to replenish the loss.

This mechanism can be clearly visualized when an input droplet containing a dye is introduced into the

immobilized droplet initially composed of clear water. As shown in Fig. 4a, the input droplet is dark and opaque before coalescence. After fusion with the immobilized droplet, the newly added volume can be easily traced within it (see Fig. 4b). The freshly delivered mass remains localized near the chamber input. In contrast, the output droplet emitted from the chamber retains the immobilized droplet's initial color.

These observations demonstrate a key advantage of the proposed system: its ability to precisely manipulate the composition of the immobilized droplet. Two main strategies can be used to adjust the concentration of a reagent within the droplet. One method involves introducing a reagent-containing droplet into the immobilized droplet, where it is diluted. The final concentration depends on the reagent concentration in the input droplet and the volume ratio between the input droplet and the immobilized droplet.

An alternative strategy involves completely replacing the liquid within the immobilized droplet by flushing the chamber with a long series of input droplets. The total volume of the input droplet series must exceed the volume of the immobilized droplet to compensate for partial mixing between the incoming fresh medium and the pre-existing contents. Under these conditions, the original contents of the immobilized droplet are completely replaced with fresh medium.

Concentration wave propagation

Another approach to manipulating the droplet contents is to propagate a concentration-gradient wave, as illustrated by the experimental images in Fig. 4. In this procedure, a reagent droplet containing a blue indicator is introduced into the immobilized droplet. The addition of the reagent generates a high-concentration wave near the inlet of the immobilized droplet. Thereafter, a series of buffer droplets is directed to the chamber. Each consecutive droplet induces translational flow through the immobilized droplet, gradually advecting the concentration wave toward the output (see Movie 2). From the perspective of a fixed position within the chamber (such as the reference points marked by red dots in Fig. 4c,d), an *in situ* observer (e.g., a cell attached to the chamber wall) experiences a time-dependent change in the concentration, characterized by an initial rise followed by a decline. This mechanism enables precisely timed stimulation by immediately exposing cells to a well-defined change in reagent concentration.

Mixing within the immobilized droplet and its enhancement

As discussed earlier for the case of a dark input droplet (see Fig. 4a,b), a portion of a new mass can be introduced into the microfluidic trap. After a new droplet flows through the trap, the added mass initially remains near the chamber inlet. It is then gradually distributed throughout the entire volume of the immobilized droplet via diffusion and convection until the droplet's contents become fully homogenized, which, in the case of small flows, can be very time-consuming.

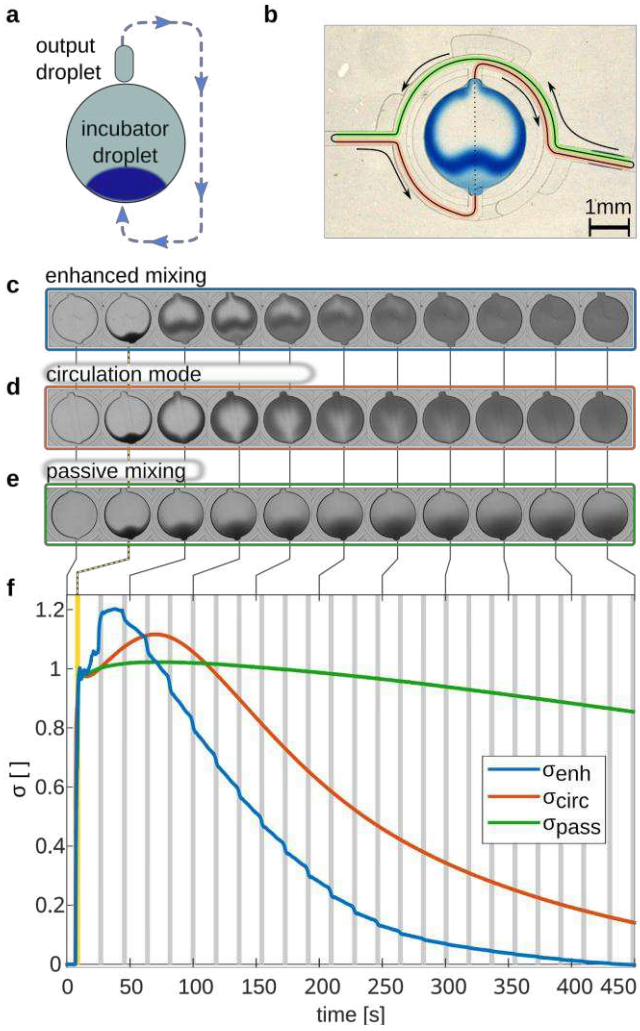


Fig. 5. *Experimental investigation of mixing within an immobilized droplet. a) Schematic illustration of the enhanced mixing procedure, in which the output droplet is recirculated as the input to induce orbiting within a closed external loop. b) Layout of the microfluidic device implementing droplet orbiting within a closed loop, with droplet trajectories indicated with: red lines for flow from left to right, green lines for flow from right to left, and black arrows for the direction of flow. c) Time-lapse sequence of images showing the dye distribution in the enhanced mixing case, where the closed-loop orbiting of a droplet facilitates mixing. d) Time-lapse sequence of images showing dye distribution in the circulation-only mixing case, where mixing is driven solely by the circulation mode. e) Time-lapse sequence of images illustrating the passive mixing of dye inside the immobilized droplet, which occurs solely by molecular diffusion. The time points shown in c)-e) correspond to those marked along the x-axis in f). f) Normalized standard deviation (σ) of the pixel intensities for the three cases: enhanced mixing (σ_{enh}), circulation-driven mixing (σ_{circ}), and passive diffusion (σ_{pass}). The gray vertical bars indicate intervals during which the orbiting droplet passes through the loop (present only in the enhanced mixing case). The yellow bar marks the injection of the dye-containing droplet (common to all three mixing conditions).*

To improve mixing and demonstrate flexibility of the microfluidic trap, we propose a procedure that creates an additional closed-loop movement of small droplets by iteratively reusing the output droplet as the input droplet (see Fig. 5a). As shown in a previous study,[33] the orbiting of a droplet within a closed trajectory in a microfluidic channel loop can be easily implemented by incorporating junctions that impose a fixed direction of droplet movement into the design. The cyclic droplet movement is achieved solely by applying an alternating flow of the CP, for example, in our case, by the forward and reverse motion of a syringe piston driven by a programmed syringe pump (see Fig. 5b). Notably, the microfluidic trap design allows for modifications (see Fig. S6) that enables an excess droplet to orbit within a loop formed by the channels surrounding the chamber (see Movie 3). This feature optimizes device size and minimizes droplet trajectory length.

To evaluate and compare mixing efficiency in both cases, we monitored the homogenization of the contents of the immobilized droplet after adding a single input droplet containing a dye. We compared the mixing enhanced by orbiting small droplets between the two sides of the immobilized droplet (see Fig. 5c) with the mixing within the droplet during the circulation mode (see Fig. 5d) and completely passive mixing (see Fig. 5e), observed when the pumps were turned off. Analysis of pixel-intensity distributions within the immobilized droplet provided a quantitative description of the temporal evolution of mixing (see Fig. 5f). The results showed that homogenization was achieved in approximately 400 s in the enhanced case, occurring significantly faster than in the non-enhanced configuration.

Preliminary experiments with cells

The presented microfluidic trap appears attractive for cell culturing in an isolated microenvironment due to its high nutrient volume that can be replaced regularly, low shear stress even in translational mode (see Fig. S7), and its ability to generate concentration waves within the immobilized droplet. Herein, we present preliminary experiments on both bacteria and adhesive cells that we found in our laboratory.

To evaluate the microfluidic trap for bacterial culturing, *Escherichia coli* was used as a model organism under three distinct perfusion regimes. The microfluidic device featured a basic trap design (see Fig. 1) with 0.5 mm chamber depth, an auxiliary inoculation channel (see Fig. S2 and S8), and integrated temperature control (see Fig. S10). While the CP flow rate was maintained at Q_{CP} = 6 mL h^{-1}, the DP flow rate was varied to assess its effect on bacterial growth. The regimes included a static control (Q_{DP} = 0.1 mL h^{-1} for 7 minutes before pump shutdown to achieve a similar starting point after flushing out inoculation media) and two continuous perfusion modes: a low flow rate (Q_{DP} = 0.05 mL h^{-1}) and a high flow rate (Q_{DP} = 0.1 mL h^{-1}).

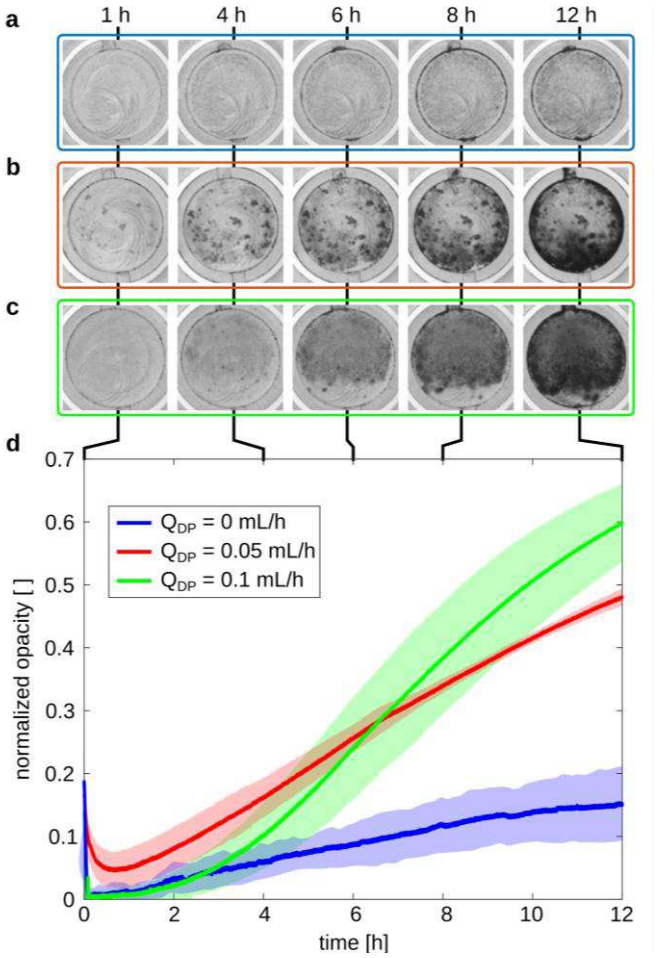


Fig. 6. *Growth of E. coli in the microfluidic trap under different medium delivery regimes: a) Snapshots of the immobilized droplet inoculated with E. coli maintained under static conditions, where the medium supply (Q_{DP} = 0.1 mL h^{-1}) was stopped 7 min after inoculation. b) Snapshots of the immobilized droplet supplied with medium at Q_{DP} = 0.05 mL h^{-1} using continuous droplet train mode. c) Snapshots of the immobilized droplet supplied with medium at Q_{DP} = 0.1 mL h^{-1} in continuous droplet train mode. d) Time evolution of immobilized droplet opacity at different medium flow rates (Q_{DP}). The curves represent the mean values from three independent experiments; shaded areas denote the standard deviation.*

The conducted experiments show that continuous perfusion significantly accelerated bacterial proliferation compared with the static control due to constant nutrient replenishment and waste removal (see Fig. 6). An initial, transient decrease in opacity was observed during early perfusion, most pronounced at the higher flow rate. Following this adaptation phase, both continuous regimes exhibited rapid exponential growth. Distinct morphological patterns emerged between the regimes: the lower flow rate promoted early, discrete bacterial aggregates that merged over time (see Fig. 6b,d), whereas the higher flow rate induced more homogeneous growth across the chamber floor (see Fig. 6c,d). These observations indicate that the rate of nutrient supply influences the spatial organization of cells. Anyway, after approximately 12 hours, the immobilized droplets were nearly filled with bacterial biofilms, and the experiments had to be stopped.

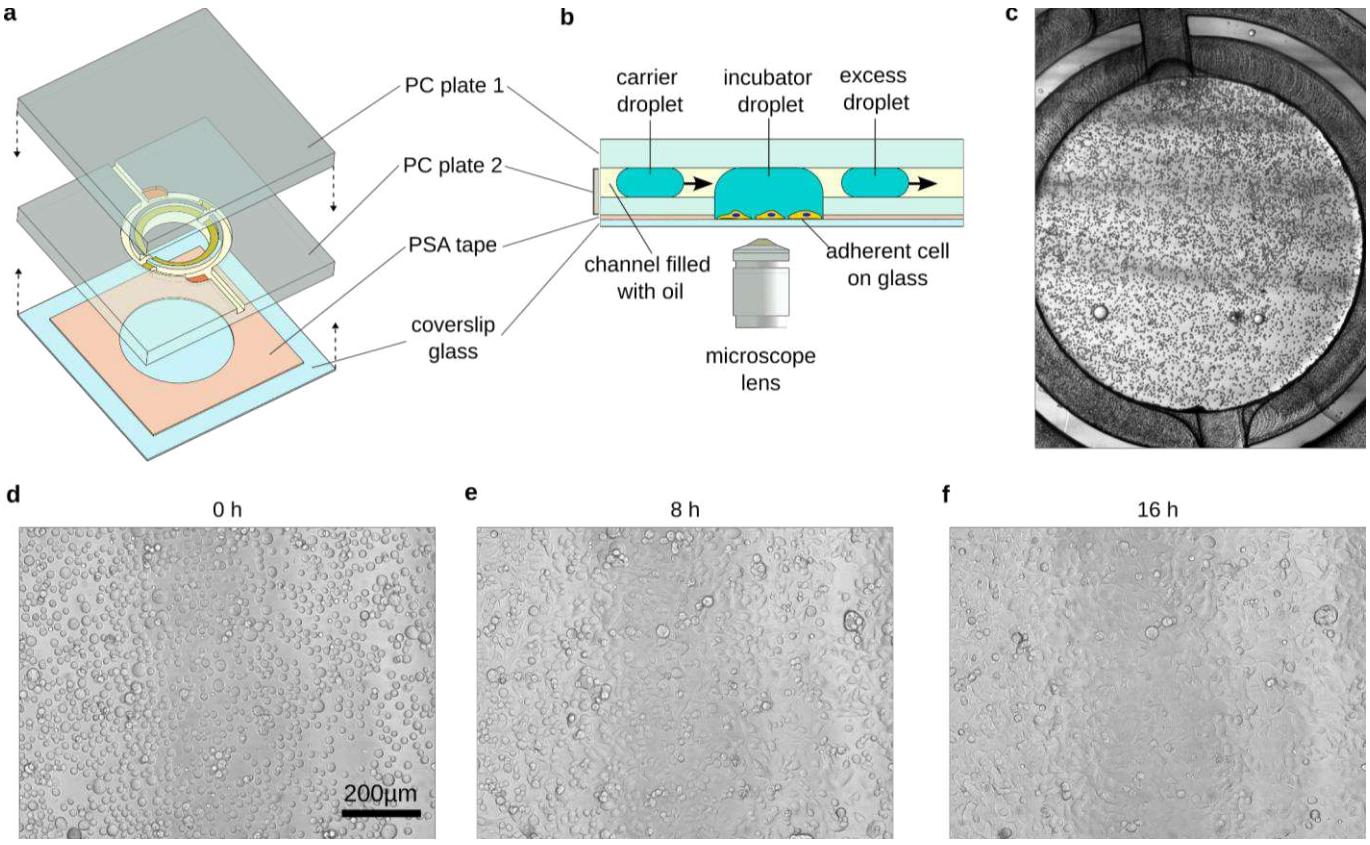


Fig. 7. *Design modifications of the microfluidic trap for adherent cell culture and test with A549 cells: a) Exploded view of the device architecture: PC plate 1 serves as a cover for the microchannels, whereas PC plate 2 contains the milled microchannels and a through-hole that defines the chamber. This opening was sealed with a PLL-coated glass coverslip affixed with PSA tape. b) Cross-sectional schematic illustrating the device operation. Input (carrier) and output (excess) droplets flow through oil-filled channels, facilitating mass exchange with the captive droplet that wets and adheres to the PLL-coated glass coverslip. Adherent cells proliferate on this glass substrate, positioned directly above the microscope objective. Element dimensions are not drawn to scale to enhance conceptual clarity. c) Overview of the whole chamber after the introduction of the cell suspension. The initial cell density was approximately 1 × 10^6 cells mL^{-1}. d-f) Representative images from Movie 5 acquired in a 1.0-mm-depth chamber with medium exchange through 3 minutes (Q_{DP} = 0.2 mL h^{-1}, Q_{CP} = 6.0 mL h^{-1}) after 5 hour from cell seeding. The A549 cells delivered to the chamber successively attach to the substrate and form a solid 2D monolayer. The scale bar applies to all snapshots.*

Since adherent cells require a suitable substrate for attachment and proliferation, several key modifications were introduced to the microfluidic trap. In particular, to improve cell adhesion, the chamber floor was replaced with a glass coverslip coated with poly-L-lysine (PLL), thereby increasing surface hydrophilicity and promoting stronger cell attachment at physiological pH. To integrate the coverslip into the device, the PC plate was drilled in the chamber area, creating an opening that was sealed from below with PSA tape, which secured the PLL-coated coverslip in place (see Fig. 7a).

To evaluate the microfluidic trap's capacity for adherent cell growth, human alveolar basal epithelial adenocarcinoma (A549) cells were observed within the modified microfluidic trap (see Fig. 7a) used

together with the adapted experimental setup (see Fig. S3, S9, and S11) at 37°C by initially replacing fresh medium in the chamber with the cell suspension (see Fig. 7b,c). Two fresh medium delivery modes were evaluated. In the continuous droplet train mode, both the DP and CP syringes operated at constant flow rates (Q_{DP} = 0.05 mL h^{-1}, Q_{CP} = 6.0 mL h^{-1}), introducing a new medium droplet into the chamber every 20 seconds. Conversely, the intermittent droplet train mode maintained periodically toggling the CP and DP syringes (Q_{DP} = 0.2 mL h^{-1}, Q_{CP} = 6.0 mL h^{-1}). During each active exchange phase lasting 2 minutes, there were resting intervals.

In the first set of experiments using a 0.5 mm-depth chamber, the continuous droplet train mode generated frequent pulses (~5 per minute) of 19.6±1.4 mPa (see Fig. S5) that repeatedly disrupted early cell adhesion, causing transient detachment. While cells eventually adapted and spread, the whole microfluidic environment influenced cellular organization (see Fig. S12). Short, intermittent intervals (30 and 60 min) reduced the frequency of disruption. Initially, they supported attachment, but the 2-minute perfusion pulses ultimately destabilized 2D adhesion, forcing cells to reorganize into free-floating 3D multicellular spheroids (see Fig. S13 and Movie 4 for 60 min intervals).

To find conditions for a stable 2D monolayer, the chamber height was increased to 1.0 mm, doubling the media volume to 7.0 µL, improving nutrient and oxygen availability, and reducing peak shear stress to 5.51±0.37 mPa, as indicated by numerical simulations in Fig. S5. However, 2D monolayers were obtained when the medium was changed once approximately 5 hours after seeding and then allowed the cells to follow a standard logistic growth curve, as in a static culture, and reach ~90% confluence within 14 hours (see Fig. 7d-f and Fig. S14). Despite increased droplet volume and reduced shear stress, we can still observe the cell response as the medium changes (see Movie 5 between 284 and 292 min).

Discussion

In this study, we present a novel microfluidic trap with a distinctive architecture inspired by the electronic Wheatstone bridge, designed to stabilize a large, stationary droplet within the trap and preserve its volume through a unique coalescence-displacement mechanism. Rather than relying on complex valve systems, we use functional geometries embedded in a microfluidic network to achieve complex two-phase fluid behavior, in which each incoming droplet coalesces with the immobilized droplet while simultaneously displacing an equivalent volume. This fluidic behavior enables high-precision medium exchange, accurate reagent dosing, and the generation of controlled concentration waves that propagate through the immobilized droplet in the chamber.

A key strength of this microfluidic trap is the substantial flexibility it provides in both geometric and operational tuning. Critical physical parameters—including the chamber diameter, depth, and shape, as well as the properties of the chamber's top or bottom surface—can be easily modified without altering the system's core operating principles. We designed the microfluidic trap based on a circular shape. However, thanks to laminar flow, the shapes of both the chamber itself and the surrounding channels can be easily modified, for example, to create an elliptical shape to achieve better flow profiles within the chamber during translational flow mode and reduce cell shock during media exchange. However, the key limitation of the

trap operation is the need to maintain a no-break-up mode at the bifurcating junction with a bypass slit,[33] to keep incoming droplets unsplit. A second limitation, for example at the maximum chamber size, is that flow through the bridge must cause less pressure than squeezing the droplet through the obstacle.[32,35]

The trap can be highly optimized for specific applications. We demonstrated that we can reduce one of the obstacles in the surrounding chamber loop, thereby enhancing rapid mixing within the chamber through faster droplet recirculation. Another minor enhancement is the addition of a block-and-brake mechanism[36] at the inlet and outlet of the chamber to keep output droplets intact, even if they are significantly longer (see Fig. S6 and Movie 6). We replaced the bottom of the chamber with PLL-coated glass. However, the bottom of the chamber can be fitted with a replaceable, adjustable-height sealing plug, coated with a droplet of biological material before being inserted into the working device. We can also achieve a pendant-droplet configuration if the chamber depth is sufficient to keep the immobilized droplet stably suspended above the chamber floor, which occurs when the CP is denser than the CP, and investigate culturing spheroids on the bottom of the pendant droplet. In addition, the chamber top can be easily replaced, as with the bottom, with, for example, a gas-permeable polymethylpentene membrane[37] that helps remove gas bubbles from the chamber and allows gas exchange directly with DP, thereby enabling the use of low-permeability CP such as mineral oil.

Because the device operates effectively across a wide range of flow rates, it relaxes the requirement for high-end fluidic control, enabling the successful use of less precise, cost-effective pumps, such as peristaltic pumps. Furthermore, the modular nature of the trap allows it to be easily integrated into larger microfluidic networks and replicated into arrays that host multiple parallel experiments using a single syringe pump for the CP and DP (see Movie 6). In addition, the microfluidic trap can be compounded with other microfluidic networks, such as a concentration-on-demand module,[38] or within the loop,[33] where oscillating CP flow delivers an output droplet from one microfluidic trap to the second, and vice versa, redirecting metabolic products from one separated culture grown in one trap to another culture grown in another.

In the presented preliminary cell experiments, we demonstrated that the proposed medium-exchange mechanism can sustain living systems with substantially different physiological requirements. Bacterial growth significantly accelerates when medium is supplied and exchanged within the immobilized droplet, enabling easier bacterial detection and the study of bacterial mechanobiology or biofilm formation in an isolated environment. For adherent cells, despite subsequent detachment during media exchange, we can also provide conditions for forming a 2D monolayer, showing that the microfluidic trap can be adapted to achieve various cell behaviors. Our trials in designed trap indicated that for A549 cells, medium exchange should not be performed too often, and to optimize the system for long-term or highly sensitive cultures fully, more detailed future studies, design optimizations, and development of new cell culture protocols are needed, specifically including optimal immobilized droplet volume, frequency and duration of medium exchange, shear-stress gradients experienced by the encapsulated cells, and gas transport rates across the chamber.

Overall, this work presents a flexible, modular microfluidic geometry with potential for handling cells, both adherent and suspended, enabling many biomedical research applications that require low shear stress, appropriate media volume, precise mass exchange, or rapid exposure to a specific substance by leveraging concentration-wave propagation, all within complex microfluidic networks. The work also presents an interesting approach to designing microfluidic devices, using standardized geometries that perform specific functions in droplet manipulation to build larger networks that enable complex and deterministic droplet behavior throughout the network, inspired by electric circuits.

Materials and methods

Liquids

For basic studies, the Continuous Phase (CP) consisted of hexadecane (Sigma-Aldrich) supplemented with 1.3% (w/w) Span 80 (Sigma-Aldrich), while the Droplet Phase (DP) consisted of distilled water. Methylene blue was added to the DP to enhance optical contrast and facilitate visualization of droplet dynamics within the chamber. To estimate flow distribution within the microfluidic network, glass particles (~5 µm) were introduced into the CP.

In experiments involving *E. coli* cultivation, the CP was replaced with HFE-7500 oil supplemented with 0.2% (w/w) biocompatible fluorosurfactant (Ran Biotechnologies). The DP consisted of Luria–Bertani (LB) medium (A&A Biotechnology S.C.) prepared with ultrapure Milli-Q® water and sterilized by autoclaving. Under sterile conditions, the LB medium was divided into two portions: one was used to prepare the bacterial inoculum. The other was drawn into an autoclaved glass syringe to generate droplets within the microfluidic device.

For mammalian cell studies, the DP consisted of Dulbecco's Modified Eagle's Medium/Nutrient Mixture F-12 (DMEM/F12), while the CP remained HFE-7500 supplemented with 0.2% fluorosurfactant. All reagents, including PBS (pH 7.4, Ca^{2+}/Mg^{2+}-free), fetal bovine serum (FBS), penicillin-streptomycin (10,000 U mL^{-1}), and TrypLE™ Express Enzyme (1X), were sourced from Thermo Fisher Scientific. To mitigate gas bubble formation during long-term microfluidic experiments, the culture medium was incubated overnight at 37 °C in sterile, vented flasks, allowing dissolved gas concentrations to equilibrate with the 5% CO_2 incubator atmosphere. Additionally, the CP was continuously aerated with 5% CO_2 during recirculation through the microfluidic system.

Cell culture

Escherichia coli (strain DH5α, Thermo Fisher Scientific) was streaked from frozen stocks onto LB agar and incubated overnight at 37 °C. A single colony was then inoculated into liquid LB medium and cultured for 5 hours at 37 °C, 180 rpm. The culture was then subcultured at a 1:75 (v/v) ratio and incubated overnight at 37 °C, 180 rpm. The resulting suspension was diluted with fresh LB medium to a final optical density (OD600) of 0.40 ± 0.02 and used to replace the initial medium immobilized in the microfluidic trap.

Adherent A549 human alveolar basal epithelial cells (Merck) were maintained in DMEM/F12 supplemented with 10% FBS and 1% penicillin-streptomycin. Cells (passages 5–20) were cultivated at 37 °C in a

humidified 5% CO_2 atmosphere, with the medium replaced every 2 days. Upon reaching 80% confluence, cells were detached using TrypLE™ Express Enzyme (1X), centrifuged at 300 × *g* for 5 min, and resuspended in pre-equilibrated DMEM/F12. This suspension was loaded into a sterile syringe and used to inoculate the immobilized droplet following the same procedure as for the bacterial experiments.

Microfluidic devices preparation

All microfluidic devices were fabricated by milling structures into polycarbonate (PC) plates (Macrolon, Bayer) using a CNC milling machine (MFG 4025 P, Ergwind) and 0.4-, 1-, or 1.5-mm 2-flute fishtail end mills (inGraph), following procedures similar to those reported in our previous studies.[32,33,35,38] While microfluidic devices (see Fig. S1 and S4) using hexadecane as the CP required no surface treatment, devices (see Fig. S2 and S3) utilizing HFE-7500 (3M™) underwent surface modification to increase hydrophobicity. Specifically, the channels were treated with Novec-1720 (3M™) through repeated filling and drying cycles at 60 °C, followed by UV sterilization and aseptic handling within a laminar flow unit.

Device architectures were adapted for specific biological experiments. Bacterial culture devices featured an auxiliary channel downstream of the trap to enable sterile inoculation without contaminating the input medium (see Fig. S2). In contrast, devices for mammalian A549 cell culture employed an asymmetric design (see Fig. S3) consisting of a thin bottom plate (0.5 or 1.0 mm) and a thicker top plate (3–5 mm). A No. 1.5 sterile glass coverslip, pre-coated with 0.1% poly-L-lysine, was attached to the bottom of the device using pressure-sensitive adhesive (PSA) tape (ARcare® 92712, Adhesives Research). This hybrid construction provided an optimal surface for cell adhesion and enabled high-resolution imaging.

Droplet generation was achieved using a block-and-brake T-junction generator,[36] ensuring constant droplet volume independent of flow rates. Adding surfactant to CP prevents droplet coalescence. To merge incoming medium droplets, electrodes were integrated near the chamber and powered by a custom high-voltage generator producing approximately 1 kV peaks at 500–1000 Hz.

Experimental setup

Optical monitoring of the microfluidic devices was performed using two distinct configurations. For observations of the basic operating mechanism and bacterial growth within the immobilized droplet (see the experimental setup in Fig. S6), a stereoscope (HSZ-645TR, Huvitz) was used. For A549 cell culture experiments (see Fig. S7), high-resolution monitoring was performed using an inverted optical microscope (DMI 3000 B, Leica) equipped with a 10x/0.25 objective (N Plan, Leica). Both optical systems utilized a UI-3274LE-C-HQ camera (IDS) for image acquisition.

Precise flow control of the DP and CP was achieved using two low-pressure syringe pumps (neMESYS, Cetoni GmbH) managed by custom Python scripts. The CP was delivered via 1 mL gas-tight glass syringes (1001TLL, Hamilton), while the DP was supplied using 2.5 mL syringes (1002TLL, Hamilton). All components were connected to the microfluidic device inlets using PTFE tubing (S2012-10, Bola GmbH). To enable long-term operation, the setup integrated 3/2-way solenoid valves (LVM095R, SMC). The system allowed for CP recirculation by drawing oil from the bottom of the collection reservoir (beneath the

settled aqueous phase) and passing it through a 0.22 µm sterile PTFE filter before re-injection.

Thermal conditions were stabilized at 37±0.1 °C using two custom-engineered solutions. For bacterial studies, the device was submerged in a 30-liter glass water tank (see Fig. S8) heated by a 90 W element and regulated by a PID controller (AR-631, APAR) connected to a 3-wire Pt100 temperature sensor (72-KFW Series, GÜNTHER). An aquarium pump enabled water circulation to ensure temperature uniformity. For mammalian cell culture, a stage-mounted heating module was employed (see Fig. S9), consisting of a copper bed and thick-film resistors controlled by a high-precision unit (TEC-1089, Meerstetter Engineering GmbH) with a 4-wire Pt100 RTD (TT-PT100A-2050-11, Tewa Sensors Sp. z o.o.).

Numerical simulations

Numerical analysis of fluid flow within the immobilized droplet was performed using a laminar, isothermal, steady-state model for incompressible, viscous, single-phase flow in Ansys Fluent 2024 R2. The three-dimensional geometry, created in Autodesk AutoCAD, was discretized via the finite volume method in Ansys Meshing, applying velocity inlet and zero-pressure outlet boundary conditions. Following grid independence validation, the final computational domains consisted of 667,625 cells for the 0.5 mm deep chamber and 1,092,450 cells for the 1.0 mm variant. These simulations resolved the pressure distributions and three-dimensional velocity fields to quantify shear stress. Post-processing in ParaView enabled visualization of flow patterns and streamlines within the immobilized droplet.

Data analysis

Video recordings were processed using ImageJ for general preprocessing and custom Python scripts that utilized OpenCV, TrackPy for image processing and droplet tracking, and OpenPIV for microparticle image velocimetry (µPIV) to estimate single-phase flow patterns. Droplet dynamics and linear velocities were quantified by analyzing the differences in surface area between consecutive thresholded binary frames. Bacterial proliferation was monitored by measuring the optical opacity of the immobilized droplet, defined as $opacity(t)=1-\frac{I(t)}{I_0}$, where $I(t)$ represents the average pixel intensity at time t, and I_0 denotes the baseline intensity of the cell-free medium, thereby correcting for background variations.

References

1. Kwon, T. *et al.* Microfluidic Cell Retention Device for Perfusion of Mammalian Suspension Culture. *Sci. Rep.* **7**, 6703 (2017).
2. Groisman, A. *et al.* A microfluidic chemostat for experiments with bacterial and yeast cells. *Nat. Methods* **2**, 685–689 (2005).
3. Hung, P. J., Lee, P. J., Sabounchi, P., Lin, R. & Lee, L. P. Continuous perfusion microfluidic cell culture array for high-throughput cell-based assays. *Biotechnol. Bioeng.* **89**, 1–8 (2005).
4. Lee, H. L. T., Boccazzi, P., Ram, R. J. & Sinskey, A. J. Microbioreactor arrays with integrated mixers

and fluid injectors for high-throughput experimentation with pH and dissolved oxygen control. *Lab. Chip* **6**, 1229–1235 (2006).

5. Balagaddé, F. K., You, L., Hansen, C. L., Arnold, F. H. & Quake, S. R. Long-Term Monitoring of Bacteria Undergoing Programmed Population Control in a Microchemostat. *Science* **309**, 137–140 (2005).
6. Rajagopalan, A. *et al.* SeqStain is an efficient method for multiplexed, spatialomic profiling of human and murine tissues. *Cell Rep. Methods* **1**, 100006 (2021).
7. Thiermann, R. *et al.* Tools and methods for high-throughput single-cell imaging with the mother machine. *eLife* **12**, RP88463.
8. Nocera, G. M. *et al.* The VersaLive platform enables microfluidic mammalian cell culture for versatile applications. *Commun. Biol.* **5**, 1–9 (2022).
9. Albrecht, D. R. *et al.* Microfluidics-integrated time-lapse imaging for analysis of cellular dynamics. *Integr. Biol.* **2**, 278–287 (2010).
10. Zhang, Y. *et al.* Dual-mode microfluidic immunostaining device for diagnostic biomarkers detection and tumor microenvironment evaluation. *Sci. Adv.* **12**, eaea2586 (2026).
11. L. Duncan, J., P. Arroyo, J. & V. Davalos, R. Microfluidics for cell therapy and manufacturing in oncology and regenerative medicine. *Lab. Chip* **26**, 1566–1587 (2026).
12. Chen, Z., Kheiri, S., Young, E. W. K. & Kumacheva, E. Trends in Droplet Microfluidics: From Droplet Generation to Biomedical Applications. *Langmuir* **38**, 6233–6248 (2022).
13. Mukherjee, M., Menon, N. V., Liu, X., Kang, Y. & Cao, B. Confocal Laser Scanning Microscopy-Compatible Microfluidic Membrane Flow Cell as a Nondestructive Tool for Studying Biofouling Dynamics on Forward Osmosis Membranes. *Environ. Sci. Technol. Lett.* **3**, 303–309 (2016).
14. Rashid, S., Ward-Bond, J., Krupin, O. & Berini, P. Non-specific adsorption of protein to microfluidic materials. *Colloids Surf. B Biointerfaces* **208**, 112138 (2021).
15. Cong, H., Xu, X., Yu, B., Liu, H. & Yuan, H. Fabrication of anti-protein-fouling poly(ethylene glycol) microfluidic chip electrophoresis by sandwich photolithography. *Biomicrofluidics* **10**, 044106 (2016).
16. Theberge, A. B. *et al.* Microdroplets in Microfluidics: An Evolving Platform for Discoveries in Chemistry and Biology. *Angew. Chem. Int. Ed.* **49**, 5846–5868 (2010).
17. Baraban, L. *et al.* Millifluidic droplet analyser for microbiology. *Lab. Chip* **11**, 4057–4062 (2011).
18. Kupikowska, B. *et al.* Influence of changes in composition of the membrane-forming solution on the structure of alginate-polyethersulfone microcapsules. *Biocybern. Biomed. Eng.* **Vol. 29**, 61–69 (2009).

19. Kupikowska-Stobba, B., Grzeczkowicz, M. & Lewińska, D. A one-step *in vitro* continuous flow assessment of protein release from core-shell polymer microcapsules designed for therapeutic protein delivery. *Biocybern. Biomed. Eng.* **41**, 1347–1364 (2021).

20. Leung, K. *et al.* A programmable droplet-based microfluidic device applied to multiparameter analysis of single microbes and microbial communities. *Proc. Natl. Acad. Sci.* **109**, 7665–7670 (2012).

21. Jakiela, S., Kaminski, T. S., Cybulski, O., Weibel, D. B. & Garstecki, P. Bacterial Growth and Adaptation in Microdroplet Chemostats. *Angew. Chem. Int. Ed.* **52**, 8908–8911 (2013).

22. Garcia-Cordero, J. L. & Maerkl, S. J. Microfluidic systems for cancer diagnostics. *Curr. Opin. Biotechnol.* **65**, 37–44 (2020).

23. Spatola Rossi, C., Coulon, F., Ma, S., Zhang, Y. S. & Yang, Z. Microfluidics for Rapid Detection of Live Pathogens. *Adv. Funct. Mater.* **33**, 2212081 (2023).

24. Jeong, H. *et al.* SCO-ph: Microfluidic Dynamic Phenotyping Platform for High-Throughput Screening of Single Cell Acidification. *Small Weinh. Bergstr. Ger.* **21**, 2504687 (2025).

25. Sart, S., Ronteix, G., Jain, S., Amselem, G. & Baroud, C. N. Cell Culture in Microfluidic Droplets. *Chem. Rev.* **122**, 7061–7096 (2022).

26. Jian, X. *et al.* Microbial microdroplet culture system (MMC): An integrated platform for automated, high-throughput microbial cultivation and adaptive evolution. *Biotechnol. Bioeng.* **117**, 1724–1737 (2020).

27. Armistead, F. J., Pablo, J. G. D., Gadêlha, H., Peyman, S. A. & Evans, S. D. Cells Under Stress: An Inertial-Shear Microfluidic Determination of Cell Behavior. *Biophys. J.* **116**, 1127–1135 (2019).

28. Sinha, N. *et al.* Microfluidic chip for precise trapping of single cells and temporal analysis of signaling dynamics. *Commun. Eng.* **1**, 18 (2022).

29. Jin, Z. *et al.* Dynamic Sessile-Droplet Habitats for Controllable Cultivation of Bacterial Biofilm. *Small Weinh. Bergstr. Ger.* **14**, e1800658 (2018).

30. Totlani, K., Hurkmans, J.-W., Gulik, W. M. van, Kreutzer, M. T. & Steijn, V. van. Scalable microfluidic droplet on-demand generator for non-steady operation of droplet-based assays. *Lab. Chip* **20**, 1398–1409 (2020).

31. Totlani, K. *et al.* Fed-Batch Droplet Nanobioreactor for Controlled Growth of Cyberlindnera (Pichia) jadinii: A Proof-Of-Concept Demonstration. *Adv. Mater. Technol.* **n/a**, 2100083.

32. Zaremba, D. *et al.* Investigations of modular microfluidic geometries for passive manipulations on droplets. *Bull. Pol. Acad. Sci. Tech. Sci.* 139-139–149 (2018).

33. Zaremba, D., Blonski, S., Marijnissen, M. J. & Korczyk, P. M. Fixing the direction of droplets in a bifurcating microfluidic junction. *Microfluid. Nanofluidics* **23**, 55 (2019).
34. Oh, K. W., Lee, K., Ahn, B. & Furlani, E. P. Design of pressure-driven microfluidic networks using electric circuit analogy. *Lab. Chip* **12**, 515–545 (2012).
35. Zaremba, D., Błoński, S. & M. Korczyk, P. Integration of capillary–hydrodynamic logic circuitries for built-in control over multiple droplets in microfluidic networks. *Lab. Chip* **21**, 1771–1778 (2021).
36. van Steijn, V. *et al.* Block-and-break generation of microdroplets with fixed volume. *Biomicrofluidics* **7**, 024108 (2013).
37. Sønstevold, L., Czerkies, M., Escobedo-Cousin, E., Blonski, S. & Vereshchagina, E. Application of Polymethylpentene, an Oxygen Permeable Thermoplastic, for Long-Term on-a-Chip Cell Culture and Organ-on-a-Chip Devices. *Micromachines* **14**, 532 (2023).
38. Zaremba, D., Blonski, S. & Korczyk, P. M. Concentration on demand – A microfluidic system for precise adjustment of the content of single droplets. *Chem. Eng. J.* **430**, 132935 (2022).

Data availability

The data supporting this article have been included as part of the Supplementary Information.

Author contributions

D.Z. conceived the design and fabricated devices, performed experiments, prepared visualizations, and wrote the manuscript; contributed to funding to a lesser degree. **B.K.-S.** contributed to cell experiments, methodology, and writing the manuscript. **S.B.** conducted numerical simulations, provided resources, contributed to fabricating devices, and helped with supervision. **P.M.K.** supervised the work, acquired funding, contributed to writing, and reviewed the manuscript.

Acknowledgements

D.Z. acknowledges support within the Preludium grant (UMO-2018/29/N/ST3/01711) of the National Science Centre, Poland. P.M.K. acknowledges support from the National Science Centre, Poland, under grant OPUS no. 2023/51/B/NZ6/02951 and from the TEAM NET grant (FENG.02.03-IP.05-0014/24) of the Foundation for Polish Science, co-financed by the European Union from the European Regional Development Fund under the European Funds for Smart Economy 2021-2027 programme.

Conflicts of interest

The authors of this work declare that they have no conflicts of interest.

Ethics approval and consent to participate

Not applicable. The A549 cell line used in this study was obtained from ATCC and cultured strictly *in vitro*.

No human subjects, fresh primary tissues, or animal models were involved in this research.

Supplementary Files

This is a list of supplementary files associated with this preprint. Click to download.

- device1.txt
- device4.txt
- Movie3.unk
- Movie1.unk
- device3.txt
- Movie6.unk
- Movie2.unk
- Movie4.unk
- device2.txt
- Movie5.unk
- SupplementaryInformation.docx